iScience, Volume *24*

Supplemental Information

Targeting CD38-dependent NAD^+ metabolism to mitigate multiple organ fibrosis

Bo Shi, Wenxia Wang, Benjamin Korman, Li Kai, Qianqian Wang, Jun Wei, Swarna Bale, Roberta Goncalves Marangoni, Swati Bhattacharyya, Stephen Miller, Dan Xu, Mahzad Akbarpour, Paul Cheresh, Daniele Proccissi, Demirkan Gursel, Jair Machado Espindola-Netto, Claudia C.S. Chini, Guilherme C. de Oliveira, Johann E. Gudjonsson, Eduardo N. Chini, and John Varga

Supplemental Information

Transparent Methods

Key Resources Table

REAGENT or RESOURCE	SOURCE	IDENTIFIER
Antibodies		
ASMA (h, m, r)*	Sigma-Aldrich	A2547
Collagen type I (h, m)	Southern Bio	1310-01
p-SMAD2/3 (h, m)	Cell Signaling	9520
CD38 (h)	Abcam	ab108403
CD38 (m)	R&D	HAF016
NNMT (h, m)	Abcam	ab119758
β-actin (h, m, r)	Sigma	A5316
Ac-Lysine	Cell Signaling	9520
P300 (h, m, r)	Santa Cruz	48343
F4/80 (m)	Cell Signaling	70076T
CD68 (h, m, r)	Abcam	Ab125212
Fibronectin-EDA	Sigma	SAB4200784

*h, human; r, rat; m, mouse

REAGENT or RESOURCE	SOURCE	IDENTIFIER
CHEMICALS, PEPTIDES, AND RECOMBINANT PROTEIN		
CD78 inhibitor (78c)	GlaxoSmithKline	GSK3010460B
Nicotinamide Riboside	ChromaDex	ASB-00014332
Recombinant human CD38	R&D system	2404-AC
Chlorhexidine gluconate	Sigma	C9394
Recombinant human TGF-β2	PeproTech	100-35B
Recombinant human TNF-α	PeproTech	300-01A
Recombinant human IL13	PeproTeck	200-13

REAGENT or RESOURCE	SOURCE	IDENTIFIER
CRITICAL COMMERCIAL ASSAYS		
NAD/NADH Quantitation Kit	Sigma-Aldrich	MAK037
NAD/NADH-Glo Assay	Promega	G9071
Hydroxyproline Assay Kit	Bio Vision	K555-100
Quick-RNA MiniPrep Kit	Zymo Research	Cat# 11-328
RNeasy Fibrous Tissue Mini Kit	QIAGEN	74704
U-PLEX biomarker Group 1 assays, SECTOR	Meso Specific Discovery	K15069L-1

REAGENT or RESOURCE	SOURCE	IDENTIFIER
EXPERIMENTAL ANIMALS		
CD38 KO mice	The Jackson Laboratory	B6.129P2-*Cd38*^{tm1Lnd}/J
C57BL6 wild-type mice	The Jackson Laboratory	
Aged mice (12, 18 month)	National Institute on Aging	

REAGENT or RESOURCE	SOURCE	IDENTIFIER
PCR PRIMERS AND REAGENTS		
mCol1A1 RT-qPCR forward 5'-AGCCGCAAAGAGTCTACATG-3'	Integrated DNA Technologies	
mCol1A1 RT-qPCR reverse: 5'-CTTAGGCCATTGTGTATGCAG-3'	Integrated DNA Technologies	
mASMA RT-qPCR forward 5'-ATGCAGAAGGAGATCACAGC-3'	Integrated DNA Technologies	
mASMA RT-qPCR reverse 5'-GTATTCCTGTTTGCTGATCCAC-3'	Integrated DNA Technologies	
mGAPDH RT-qPCR forward 5'-ATCTTCTTGTGCAGTGCCAGC-3'	Integrated DNA Technologies	
mGAPDH RT-qPCR reverse 5'-GTTGATGGCAACAATCTCCAC-3'	Integrated DNA Technologies	
hFn-EDA RT-qPCR forward 5’TAAAGGACTGGCATTCACTGA3’	Integrated DNA Technologies	
hFn-EDA RT-qPCR reverse 5’ GTGCAAGGCAACCACACTGAC3’	Integrated DNA Technologies	
hCol1A1 RT-qPCR forward 5'-TGGTGTGCAAGGTCCC-3'	Integrated DNA Technologies	
hCol1A1 RT-qPCR reverse 5'-CATTCCCTGAAGGCCAG-3'	Integrated DNA Technologies	

hASMA RT-qPCR forward 5'-CAGGGCTGTTTTCCCATCCAT-3'	Integrated DNA Technologies	
hASMA RT-qPCR reverse 5'-GCCATGTTCTATCGGGTACTTC-3'	Integrated DNA Technologies	
hGAPDH RT-qPCR forward 5'-CATGAGAAGTATGACAACAGCCT-3'	Integrated DNA Technologies	
hGAPDH RT-qPCR reverse 5'-AGTCCTTCCACGATACCAAAGT-3'	Integrated DNA Technologies	

ANTI-MOUSE ANTIBODIES USED FOR FLOW CYTOMETRY		
REAGENTS	**SOURCE**	**IDENTIFIER (clone)**
CD45 V500	BD Biosciences	30-F11
Siglec F Alexa 647	BD Biosciences	E50-2440
CD11c APC-Cy7	BioLegend	N418
Ly6C PE	BioLegend	HK1.4
CD80 BV605	BioLegend	16-10A1
CD86 BV605	BioLegend	GL-1
CD11b BV421	BioLegend	M1/70
Cd64 PE-Cy7	BioLegend	X54-5/7
Ly6G PerCP5.5	BioLegend	1A8
I-A/I-E FITC	BioLegend	M5/114.15.2
CD3 Alexa 700	BioLegend	500A2
CD44 APC-Cy7	BioLegend	IM7
TCR$\gamma\delta$ APC	BioLegend	GL3
CD45 V500	BioLegend	30-F11
CD69 BV605	BioLegend	H1.2F3
CD62L PE-Cy7	BioLegend	MEL-14
CD25 PE	BioLegend	3C7
CD11b V500	BioLegend	M1/70
CD38 PE-Cy7	BioLegend	90

MARCO APC	BioLegend	FAB2956A
CD8 Alexa700	BioLegend	53-6.7
FoxP3 Per CP-Cy5.5	BioLegend	FJK-16s
iNOS PE-Cy7	eBioscience	25-5920-80
EgR2 PE	eBioscience	12-6691-82
CD206 APC	eBioscience	141708

Method Details

Mouse fibrosis models

Bleomycin model: Animal protocols were institutionally approved by the Animal Care and Use Committees of Northwestern University. We used 18 months-old C57BL/6J female wild-type (National Institute on Aging, NIA) and 12 months-old CD38KO mice on the C57BL/6 background (B6.129P2-*CD38*^{tm1Lnd}/J, Jackson laboratory) as previously described (Camacho-Pereira et al., 2016, Cockayne et al., 1998, Guedes et al., 2006). For *in vivo* experiments, mice were randomized to receive vehicle, bleomycin, or bleomycin in combination with CD38 inhibitor 78c (GlaxoSmithKline, Philadelphia, PA) (Haffner et al., 2015). Mice were fed a standard chow diet or chow supplemented with nicotinamide riboside (NR, 3g/kg chow) (ChromaDex, Irvine, CA). 78c was dissolved in 0.5% (w/v), K-15 HPMC (Sigma H7509), and 0.1% (w/v) Tween 80 and administered by daily gavage feeding (30 mg/kg) (Tarrago et al., 2018, Haffner et al., 2015). Mice were given daily subcutaneous (s.c.) injections of PBS or bleomycin (10 mg/kg, Teva Pharmaceuticals, North Wales, PA) in parallel for 14 d. Mice were sacrificed on day 21, and lesional skin and lungs were harvested. Tissue collagen content was determined by hydroxyproline assays (Bhattacharyya et al., 2018a).

Peritoneal membrane fibrosis: Wild-type (from NIA) and CD38 null C57BL/6J male mice were used. Peritoneal membrane fibrosis was induced by alternate-daily i.p. injections (0.3ml, 10 injections) of 0.1% chlorhexidine gluconate (CG, Sigma, C9394) dissolved in 15% ethanol/PBS, while mice in the control group received i.p. injections of 15% ethanol/PBS solvent only. Mice were maintained on a diet of chow supplemented with NR (3 g/kg chow), and daily oral gavage with 78c (30 mg/kg). At day 19, mice were sacrificed, and peritoneal tissues were carefully

dissected, and peritoneal membrane thickness (submesothelial compact zone superficial to the abdominal wall muscles) was determined (Bhattacharyya et al., 2018a, Yokoi et al., 2012) .

Cell cultures

Primary cultures of human dermal fibroblasts were established by explantation from neonatal foreskin or from adult forearm skin biopsies of SSc patients or matched healthy control subjects (Bhattacharyya et al., 2016). Primary dermal fibroblasts were also established from wild-type and CD38-null mice. Early–passage (<5) fibroblasts were grown in monolayers in 6-well plastic dishes or 100 mm plates (Corning Incorporated) and studied at early confluence (Bhattacharyya et al., 2013). Cultures of mouse and human fibroblasts were maintained in DMEM supplemented with 10% FBS (Thermo Fisher Scientific), 1% vitamin solutions, 2 mM L-glutamine, and 120 Units/ml penicillin and streptomycin (Lonza, Alpharetta, GA). To test fibrotic response, confluent fibroblasts were incubated in serum-free media containing 10 ng/ml TGF-β2 (Peprotech, Rocky Hill, NJ, 100-21) and 0.1% BSA (Sigma, St. Louis, MO). Indicated reagents were added 2 h prior to TGF-β2 (Chavez et al., 2011). To induce CD38 in fibroblasts, human skin fibroblasts at exponential growth in complete DMEM culture medium were co-incubated with TNF-α (10ng/ml), TGF-β2 (10ng/ml) or IL-13(10ng/ml) for 24 hours.

To generate bone marrow-derived macrophage (BMDM), femurs and tibias from wild type and CD38-null mice were harvested and cultured as previously described (Jablonski et al., 2016). Briefly, isolated cells were incubated in Dulbecco's Modified Eagle Media (DMEM, Mediatech, Herndon, VA) supplemented with 10% heat-activated fetal bovine serum (FBS) (Life Technologies, Grand Island, NY), 1% penicillin/streptomycin, 1% glutamine, and 20% L929 cell

culture supernatant which contains macrophage colony stimulating factor. On day 8, cells were re-seeded into 24-well plates, and incubated with media alone (unstimulated M0 condition) or M1-activated with LPS (100 ng/ml, Sigma-Aldrich L2880) + mIFN-γ (20ng/mL, R&D 485-MI/CF) or alternatively/M2-activated with IL-4 (20 ng/mL, R&D 404-ML/CF) + mIL-13 (20 ng/ml, R&D 413-ML/CF) for 24 hours. CD38i (78c, 0.5μM) and NR (100 μM) were added after reseeding, and cells were harvested at the indicated time-points for RNA and protein isolation or flow cytometric analysis.

RNA isolation and qPCR analysis

Total RNA from cultured human and mouse fibroblasts, macrophages or mouse tissues was isolated by Quick RNA miniprep kit (Zimo Research, Irvine, CA, 11-328) or /by RNeasy Fibrous tissue mini kits (Qiagen, Germantown, MD, 74704). Reverse transcription of RNA to cDNA was performed using Supermix (cDNA Synthesis Supermix; Quanta Biosciences, Beverly, MA) as described (Bhattacharyya et al., 2016). Amplification products (50 ng) were amplified using SYBR Green PCR Master Mix or TagMan gene expression assay (Applied Biosytems, Foster city, CA) on an Applied Biosystems 7500 Prism Sequence Detection System. Gene expression was normalized to internal GAPDH, and -fold change was calculated (Bhattacharyya et al., 2018b). Primer sequences are shown in Key Resources Table.

Immunoblotting

At the end of the experiments, cells or mouse tissues were harvested, whole cell lysates prepared, and equal amounts of proteins subjected to Western blot analysis as described

(Bhattacharyya et al., 2013). Primary and secondary antibodies used are listed in Key Resources Table (Antibodies). Band intensities in Western blot were photo scanned and quantitated using ImageJ (NIH) and normalized to β-actin or GAPDH.

Transient transfection and luciferase assays

Subconfluent foreskin fibroblasts were transiently transfected with $(SBE)_4$-luc plasmids using SuperFect transfection reagent (Qiagen, Germantown, MD). Following 24 h incubation, cultures were harvested and whole cell lysates were assayed for their luciferase activities (Bhattacharyya et al., 2016). All experiments were performed in triplicates.

Immunofluorescence confocal microscopy

Foreskin fibroblasts were seeded on glass coverslips and studied by immunofluorescence as described (Bhattacharyya et al., 2018a, Fang et al., 2016). The antibodies used are described in Key Resource Table (Antibodies). Fibroblasts at 80% confluence were fixed in 3.7% paraformaldehyde, permeabilized, and incubated with antibodies to α-SMA (MilliporeSigma, St. Louis, MO) or phospho-Smad2 (Cell Signaling Technology Inc., Danvers, MA, 3018) at 1:100 dilution, followed by Alexa Fluor–labeled secondary antibodies (Invitrogen, Norcross, GA). Nuclei were counterstained with DAPI. Subcellular distribution of immunofluorescence was evaluated under an immunofluorescence microscope or Zeiss UV Meta 510 confocal microscope or a Nikon C2 or A1Si confocal microscope and quantitated using Image J.

Determination of NAD^+ consumer/biosynthesis enzyme expression in SSc skin biopsies and in murine models

To determine levels of NAD^+ consumer and biosynthesis enzymes in SSc, we queried publicly available multiple genome-wide skin biopsy-based transcriptome datasets. First, we queried (GSE76886 https://www.ncbi.nlm.nih.gov/geo/query/acc.cgi?acc=GSE76886), comprised of baseline skin biopsies from 68 SSc patients (12 limited and 56 diffuse cutaneous disease) and 22 healthy controls. Two additional datasets (PRESS and SPARC) from independent patient cohorts were used to validate the results. GSE130955 (PRESS) cohort (https://www.ncbi.nlm.nih.gov/geo/query/acc.cgi?acc=GSE130955) analyzed global gene expression from skin biopsies of 48 patients with early diffuse cutaneous SSc and 33 matched healthy controls (Skaug et al., 2020). The SPARC cohort used RNA-seq generate genome wide transcriptome profiles from 14 healthy control and 20 SSc (6 lcSSc and 14 dcSSc) skin biopsies (Roberson et al., 2016). Transcript levels in each biopsy were centered on their median values across all arrays.

To correlate gene expression levels to modified Rodnan skin score (MRSS) in each biopsy, profibrotic signaling pathways were analyzed using Pearson's correlation coefficient test. Pathway gene signatures of TGF-β and PDGF were defined as all genes ≥ 2-fold up- or down-regulated across all of their corresponding 12 and 24 hour time points in cultured human dermal fibroblasts relative to untreated controls (Johnson et al., 2015). SIRT1 signature genes were extracted from published datasets (Beane et al., 2012). SIRT1 pathway scores, defined as Pearson's correlation coefficients of each pathways, were used to quantify the contribution of a specific pathway to the gene expression within a given patient. (Johnson et al., 2015). Mann

Whitney *U* test and 1-way ANOVA method were used to analyze differences between groups. Additionally, we queried skin gene expression data from mice with experimentally-induced scleroderma (GSE71999 (Sargent et al., 2016), and GSE13289) (https://www.ncbi.nlm.nih.gov/geo/query/acc.cgi?acc=GSE132869).

Histology and Immunohistochemistry

4-μm thick sections of formalin-fixed, paraffin-embedded skin biopsy samples from SSc patients, healthy subjects or from mouse skin tissue and lungs were analyzed by immunohistochemistry, as described (Bhattacharyya et al., 2018a). Demographic and clinical features of Healthy subject and SSc patient skin biopsies used for CD38 expression were listed in Table 1. Slides were incubated with anti-mouse CD38 (Abcam, Cambridge, MA, ab230153), anti-mouse or human SMA (Sigma, St. Louis, MO, A2547), F4/80 (Cell Signaling, 70076T) and mouse CD68 (Abcam, ab125212), human CD38 (Abcam, ab108403) antibodies, or isotype-matched control IgG (eBioscience, San Diego, CA) followed by HRP-conjugated secondary antibody which was visualized with diaminobenzidine substrate, and counterstained with hematoxylin. Immunopositive cells were counted in 5 randomly selected high-power fields (hpf, 40X objective) per biopsy specimen by an observer in a blinded manner (Fang et al., 2016). One-way ANOVA was used for statistic significant analysis.

Supplemental Table 1. Demographic and clinical features of subjects (skin biopsies used for IHC analysis, related to Figure 1H and 1I).

Identifier	Age (years)	Sex	Race	Diagnosis	Disease duration (months)	MRS*
SPARC_SSc_02	31	Female	Hispanic	dcSSc	40	6
SPARC_SSc_19	36	Female	Hispanic	dcSSc	24	17
SPARC_SSc_15	30	Male	White	lcSSc	28	17
SPARC_SSc_16	45	Female	Black	dcSSc	56	11
SPARC_SSc_05	60	Male	White	lcSSc	44	6
SPARC_SSc_31	60	Female	White	dcSSc	12	36
SPARC_SSc_06	69	Male	White	dcSSc	12	41
SPARC_SSc_07	50	Female	White	dcSSc	9	24
SPARC_SSc_10	40	Female	White	dcSSc	72	16
SPARC_SSc_11	64	Female	White	dcSSc	8	33
SPARC_NORM_08	28	Female	Hispanic	Control	N/A	N/A
RegNorm_1015	35	Female	Hispanic	Control	N/A	N/A
SPARC_NORM_05	26	Male	White	Control	N/A	N/A
RegNorm_1026	56	Male	White	Control	N/A	N/A

*dcSSc, diffuse cutaneous SSc; MRSS, modified Rodnan skin score (0-51)

Measurement of skin and lung fibrosis

Dermal thickness was determined at 5 randomly selected sites as previously described (Bhattacharyya et al., 2016). Ashcroft score, reflecting both severity and extent of lung fibrosis (Ashcroft et al., 1988) was determined in a blinded manner by a pulmonary pathologist.

Measurement of NAD metabolism

Levels of NAD^+ in confluent human fibroblast cultures and mouse skin, lung and liver were measured using NAD/NADH quantification kits according to manufacturer's instructions (Sigma-Aldrich, MAK037). NAD^+ levels in serum were measured using NAD/NADH Glo Assay kit (Promega, G9071) Tissue levels of NAD^+ and its metabolites were also determined by Ultra-performance

Liquid Chromatography (UPLC)-Mass Spectrometry (de Oliveira et al., 2018, Kanamori et al., 2018). In brief, harvested tissues were immediately immersed in 10% TCA (Sigma, St. Louis, MO, T6399), snap frozen in liquid nitrogen, and preserved at -80^{o}C. Samples were then thawed on ice and levels of NAD^{+}, nicotinamide mononucleotide (NMN), and nicotinamide riboside (NR) were determined using cycling assay employing UPLC-Mass spectrometry (Camacho-Pereira et al., 2016).

Microcomputed lung tomography

Lung computed tomography (CT) images were acquired using a Mediso NANOSCAN8 PETCT system (Mediso USA) using 50KeV energy, an exposure time of 300 msec for each projection for a total of 710 projections per mouse. 3D images were reconstructed with a final isotropic spatial resolution of 100 micrometers. Mice were maintained under anesthesia delivered through a nose cone with isofluorane mixed with 100% oxygen in a supine position. 3-D images were exported off-line in DICOM format and analyzed using threshold segmentation algorithms provided in ITK-SNAP software (Yushkevich et al., 2006). Varying Hounsfeld units (HU) threshold windows were used to differentiate healthy tissue from fibrotic lung tissue. Total lung volume for each mouse was determined using a threshold window that enabled masking of whole lung and removal of surrounding tissue (HU 1000-500). Two thresholds were then used to acquire “normal tissue” (-1000 - -100 HU) and “abnormal/fibrotic tissue” (-100 - +500 Hu). The three sets of volumetric data corresponding to different threshold windows were generated for each of the mice scanned for each cohort. The control group (i.e. no fibrosis) was used as a standard reference value to generate the index factors (lung fibrotic index).

Flow cytometry

Flow cytometry analysis of the skin, lungs and spleen was performed as described (Misharin et al., 2013, Prasad et al., 2018, Bharat et al., 2016). Briefly, at sacrifice organs were harvested, perfused with PBS and cut into small pieces and processed in digestion buffer (1 mg/ml of Collagenase D and 0.1 mg/ml DNase I, both from Roche, Indianapolis, IN), using GentleMACS dissociator (Miltenyi). Homogenized tissues were passed through 40-μm nylon mesh to obtain a single-cell suspension. The red blood cells were lysed using BD Pharm Lyse (BD Biosciences, Cat# 555899). Cells were incubated with mouse Fc-block (Cat# 553142, BD Biosciences, San Jose, CA) followed by appropriate antibody cocktails. These antibodies included CD45, CD11b, CD11c, Ly6C, Ly6G, MHC II, CD80, CD86, B220, CD3, CD4, CD8, and CD38 (all from BioLegend, San Diego, CA, and eBioscience). Live/dead fixable blue (Cat# L-23105, Invitrogen, Carlsbad, CA) was added to the cells thereafter to label dead cells prior to cell fixation with 0.5% formaldehyde diluted with PBS. Each incubation step was performed at 4^{o}C for 30 minutes in dark. Antibodies are listed in Key Resources with the antigen, conjugated fluorophore, and clone specified. A 6-laser Fortessa flow cytometer (BD Biosciences) was used to enumerate cell populations and the data was analyzed using FlowJo software (TreeStar, Ashland, OR). For *ex vivo* differentiation assays, bone marrow-derived macrophages were fixed and permeabilized using thexP3 staining buffer kit s(eBioscience), and immunostained with antibodies to inducible nitric oxide synthase (iNOS), EgR2, and CD206 (Key Resources Table). Cells were acquired on a BD Fortessa and analyzed using BD FlowJo version 9. As controls, fluorescence minus one (FMO) was used to place the gates for analysis.

Statistics

Data are presented as means ± SEM. Two-tailed Student's *t* test or Mann Whitney *U* test was used for comparisons between 2 groups. If experiment involved more than three groups, 1-way ANOVA followed by Tukey analysis was used to examine for statistical significance. The Chi Square analysis was used for categorical variables. A *p* value less than 0.05 denoted the presence of statistically significant difference. The Pearson correlation for continuous variables and the Spearman correlation for ordinal variables were used to evaluate relationships between two variables. Data were analyzed and graphs were created using GraphPad prism (GraphPad Prism Software version 7.03, GraphPad Software Inc.).

Study approvals

All animal studies were conducted in accordance with NIH guidelines for the care and use of laboratory animals and protocols were approved by the IACUC of Northwestern University. Studies involving human subjects were approved by the IRB of Northwestern University, and all participants provided written informed consent.

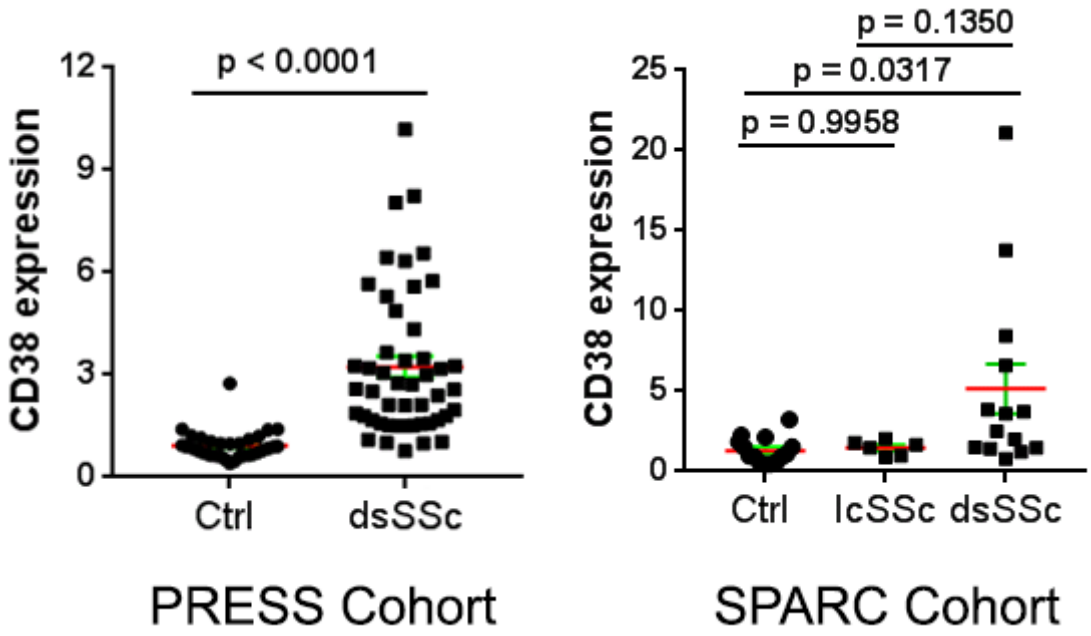

Figure S1 (related to Figure 1). Significantly elevated CD38 mRNA in SSc skin biopsies in two independent patient cohorts. The PRESS cohort dataset (GSE130955) comprises global gene expression data from skin biopsies of 48 patients with early diffuse cutaneous SSc and 33 matched healthy controls. The SPARC cohort comprises global gene expression data (RNA-seq) from skin biopsies of 20 patients with SSc (6 lcSSc and 14 dcSSc) and 14 healthy controls. Error bars, means ± SEM.

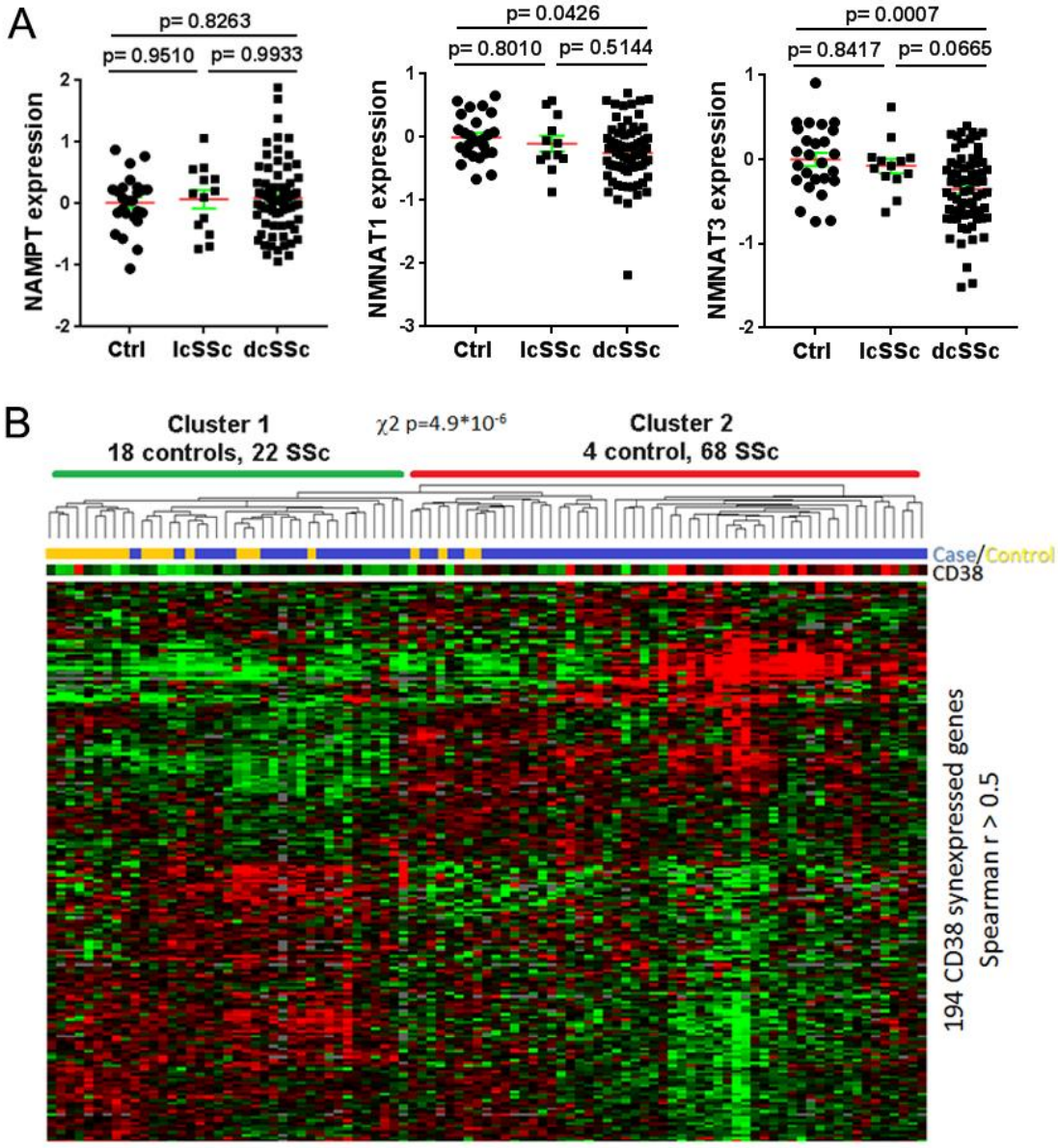

Figure S2 (related to Figure 1). Interrogating skin biopsy transcriptomes: healthy control and SSc skin biopsies. Gene expression from SSc and control individuals' skin was assessed (GEO accession GSE76886). (A) Expression of NAD^+ salvage pathway enzymes NAMPT, NMNAT1, and NMNAT3 in healthy controls, lcSSc and dcSSc biopsies. Error bars are means ± SEM. (B) A 194-gene CD38 co-expression gene module (genes with Spearman correlation r>0.5 with CD38) is able to discriminate SSc from healthy control skin biopsies using hierarchical clustering.

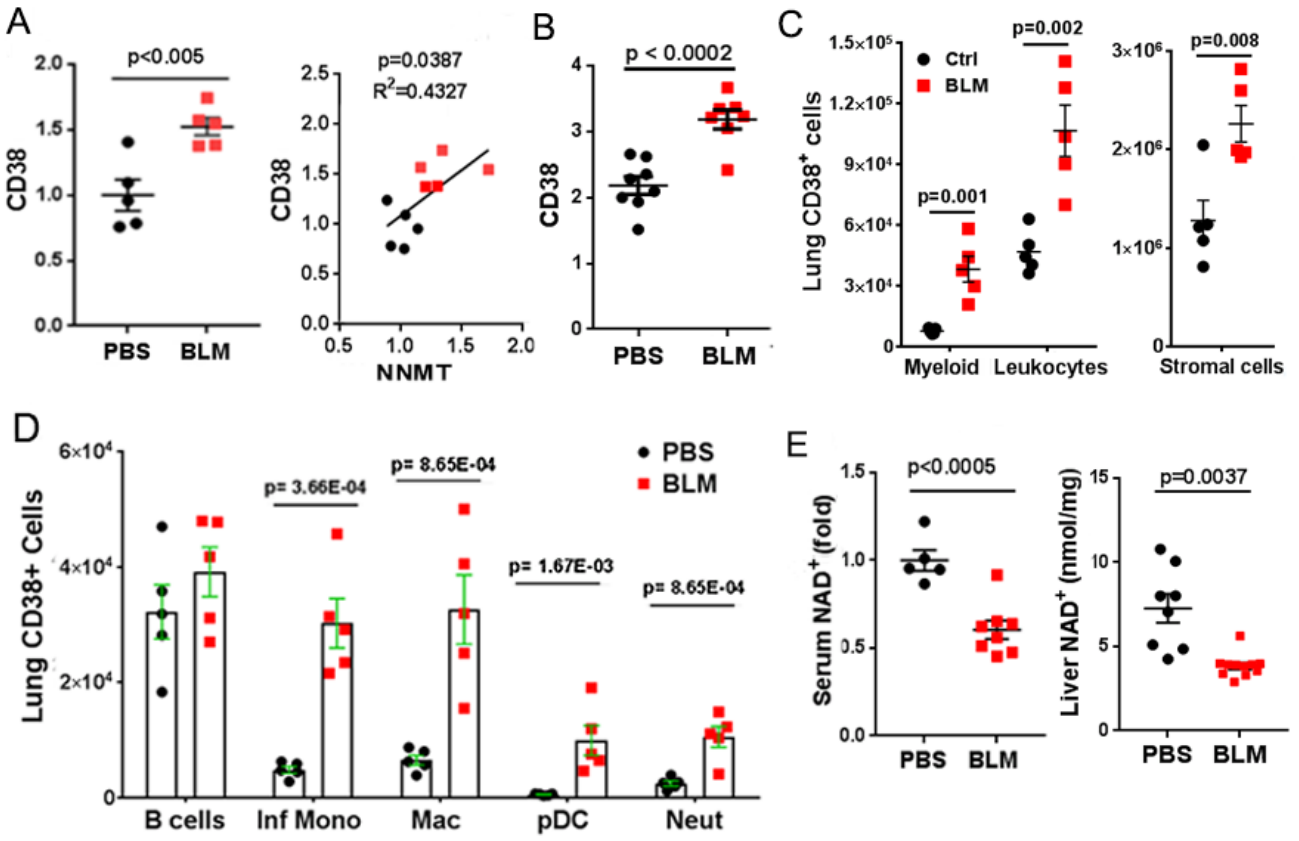

Figure S3. Elevated CD38 associated with reduced NAD⁺, related to Figure 1. (A) Elevated CD38 mRNA levels in skin from bleomycin-treated mice (d 21). Analysis of dataset GSE71999. Right panel, CD38 levels correlated with NNMT levels in same skin biopsies. (B) Elevated CD38 mRNA in an independent mouse experiment (GSE13289). (C), (D) Flow cytometry of lung cells from bleomycin-treated and control mice. Elevated numbers of CD38+ hematopoietic (left panel) and stromal (right panel) cell populations. (D) CD38-positive inflammatory cell subpopulations. (E) Levels of circulating and tissue (liver) NAD^+ in bleomycin-treated mice (NAD^+ measured as described under Methods). Bar graphs are means ± SEM.

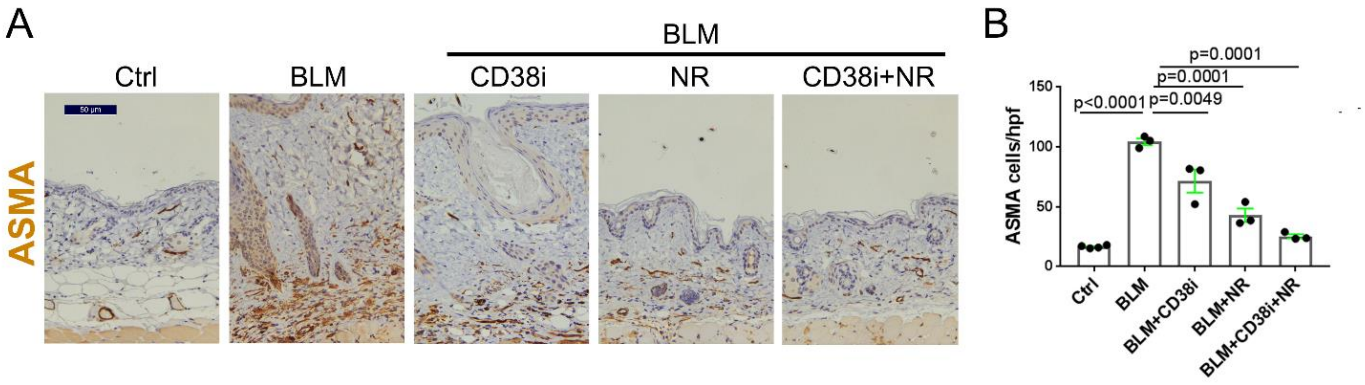

Figure S4 (related to Figure 3). **CD38 inhibitor and NR supplementation reduced skin myofibroblast accumulation in bleomycin-treated mice.** (A) Immunohistochemistry of skin from mice treated with NR supplementation and 78c (CD38i) alone or in combination using antibodies against alpha smooth muscle actin (ASMA); representative images. Scale bar length: 50 μm. (B) Quantification of myofibroblasts within the lesional dermis. ASMA-positive interstitial cells were counted in 5 randomly selected high-power fields (hpf, 40 x objective, scale bar = 50 μm) per slide. Bars are means ± SEM (one-way ANOVA).

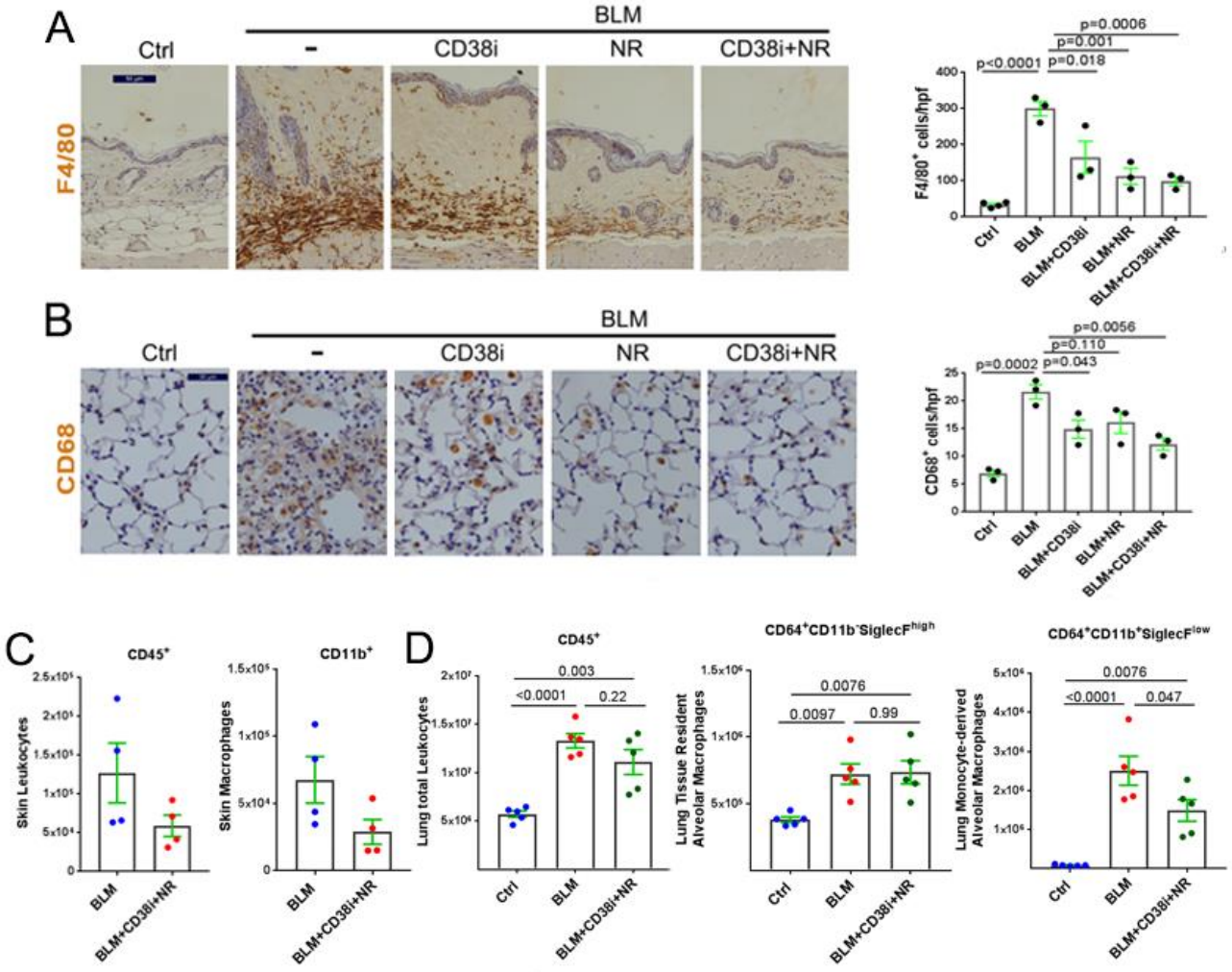

Figure S5 (related to Figure 3). CD38 inhibitor 78c and NR attenuated bleomycin-induced skin and lung inflammation. C57/BL6 mice were treated with s.c. bleomycin and CD38 inhibitor (30 mg/kg by gavage) plus NR supplementation (3g/kg chow). Mice were sacrificed at day 21 and skin and lungs harvested for analysis. (A and B) Immunohistochemistry of skin (A) and lung (B) using antibodies to F4/80 or CD68. Representative images (left panels); scale bar length: 50 μm. quantification of immunopositive cells (right panels). (C and D) Flow cytometry analysis of inflammatory cells in skin and lungs. Immunopositive cells were counted in 5 randomly selected high-power fields (hpf, 40 x objective) per slide. Bars are means ± SEM.

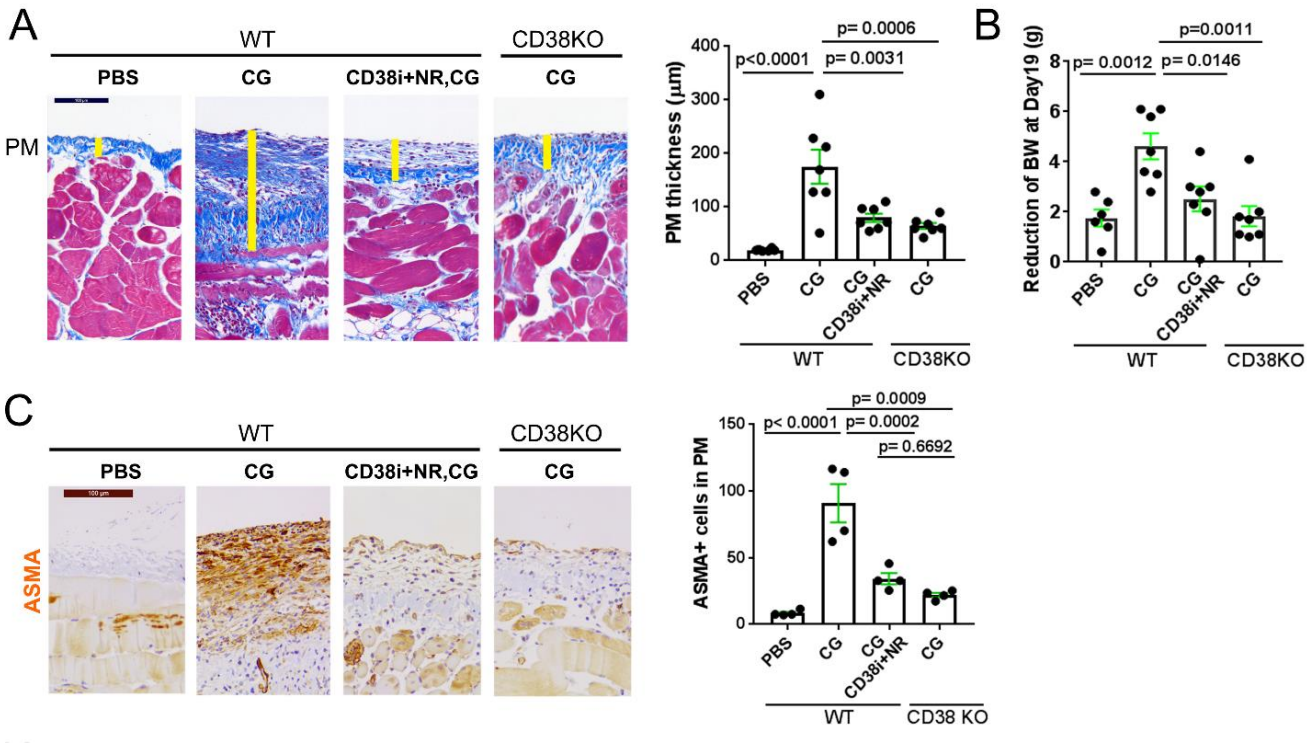

Figure S6 (related to Figure 3). Genetic or pharmacological targeting of CD38 ameliorates peritoneal fibrosis. 15 month-old wild-type and CD38 null C57BL/6J male mice were used. Peritoneal membrane fibrosis was induced by alternate-daily i.p. injections 0.1% chlorhexidine gluconate for 19 days. Mice were maintained on standard chow or NR-supplemented chow diet (3g/kg) plus daily oral gavage with 78c (30 mg/kg BW). Mice were sacrificed at day 19, and parietal peritoneal membranes were harvested for analysis. (A) Left panel, Masson's trichrome stain, and representative images. Right panel, submesothelial compact zone thickness was indicated by yellow bar. (B) Weight loss of mice groups. (C) Immunostaining with antibodies to ASMA. Representative images (left). Scale bar length in (A and C): 100 μm. Quantitation of F4/80-positive cells in the peritoneal membrane (right panel). All bar graphs are means ± SEM. One-way ANOVA followed by Tukey post hoc tests was used for statistic significant analysis.

Supplemental References

Ashcroft, T., Simpson, J. M. & Timbrell, V. 1988. Simple method of estimating severity of pulmonary fibrosis on a numerical scale. *J Clin Pathol,* 41**,** 467-70.

Beane, J., Cheng, L., Soldi, R., Zhang, X., Liu, G., Anderlind, C., Lenburg, M. E., Spira, A. & Bild, A. H. 2012. SIRT1 pathway dysregulation in the smoke-exposed airway epithelium and lung tumor tissue. *Cancer Res,* 72**,** 5702-11.

Bharat, A., Bhorade, S. M., Morales-Nebreda, L., Mcquattie-Pimentel, A. C., Soberanes, S., Ridge, K., Decamp, M. M., Mestan, K. K., Perlman, H., Budinger, G. R. & Misharin, A. V. 2016. Flow Cytometry Reveals Similarities Between Lung Macrophages in Humans and Mice. *Am J Respir Cell Mol Biol,* 54**,** 147-9.

Bhattacharyya, S., Kelley, K., Melichian, D. S., Tamaki, Z., Fang, F., Su, Y., Feng, G., Pope, R. M., Budinger, G. R., Mutlu, G. M., Lafyatis, R., Radstake, T., Feghali-Bostwick, C. & Varga, J. 2013. Toll-like receptor 4 signaling augments transforming growth factor-beta responses: a novel mechanism for maintaining and amplifying fibrosis in scleroderma. *Am J Pathol,* 182**,** 192-205.

Bhattacharyya, S., Wang, W., Morales-Nebreda, L., Feng, G., Wu, M., Zhou, X., Lafyatis, R., Lee, J., Hinchcliff, M., Feghali-Bostwick, C., Lakota, K., Budinger, G. R., Raparia, K., Tamaki, Z. & Varga, J. 2016. Tenascin-C drives persistence of organ fibrosis. *Nat Commun,* 7**,** 11703.

Bhattacharyya, S., Wang, W., Qin, W., Cheng, K., Coulup, S., Chavez, S., Jiang, S., Raparia, K., De Almeida, L. M. V., Stehlik, C., Tamaki, Z., Yin, H. & Varga, J. 2018a. TLR4-dependent fibroblast activation drives persistent organ fibrosis in skin and lung. *JCI Insight,* 3**,** e98850.

Bhattacharyya, S., Wang, W., Tamaki, Z., Shi, B., Yeldandi, A., Tsukimi, Y., Yamasaki, M. & Varga, J. 2018b. Pharmacological Inhibition of Toll-Like Receptor-4 Signaling by TAK242 Prevents and Induces Regression of Experimental Organ Fibrosis. *Front Immunol,* 9**,** 2434.

Camacho-Pereira, J., Tarrago, M. G., Chini, C. C., Nin, V., Escande, C., Warner, G. M., Puranik, A. S., Schoon, R. A., Reid, J. M., Galina, A. & Chini, E. N. 2016. CD38 Dictates Age-Related NAD Decline and Mitochondrial Dysfunction through an SIRT3-Dependent Mechanism. *Cell Metab,* 23**,** 1127-39.

Chavez, S. A., Martinko, A. J., Lau, C., Pham, M. N., Cheng, K., Bevan, D. E., Mollnes, T. E. & Yin, H. 2011. Development of beta-amino alcohol derivatives that inhibit Toll-like receptor 4 mediated inflammatory response as potential antiseptics. *J Med Chem,* 54**,** 4659-69.

Cockayne, D. A., Muchamuel, T., Grimaldi, J. C., Muller-Steffner, H., Randall, T. D., Lund, F. E., Murray, R., Schuber, F. & Howard, M. C. 1998. Mice deficient for the ecto-nicotinamide adenine dinucleotide glycohydrolase CD38 exhibit altered humoral immune responses. *Blood,* 92**,** 1324-33.

De Oliveira, G. C., Kanamori, K. S., Auxiliadora-Martins, M., Chini, C. C. S. & Chini, E. N. 2018. Measuring CD38 Hydrolase and Cyclase Activities: 1,N(6)-Ethenonicotinamide Adenine Dinucleotide (epsilon-NAD) and Nicotinamide Guanine Dinucleotide (NGD) Fluorescence-based Methods. *Bio Protoc,* 8**,** e2938.

Fang, F., Marangoni, R. G., Zhou, X., Yang, Y., Ye, B., Shangguang, A., Qin, W., Wang, W., Bhattacharyya, S., Wei, J., Tourtellotte, W. G. & Varga, J. 2016. Toll-like Receptor 9 Signaling Is Augmented in Systemic Sclerosis and Elicits Transforming Growth Factor beta-Dependent Fibroblast Activation. *Arthritis Rheumatol,* 68**,** 1989-2002.

Guedes, A. G. P., Paulin, J., Rivero-Nava, L., Kita, H., Lund, F. E. & Kannan, M. S. 2006. CD38-deficient mice have reduced airway hyperresponsiveness following IL-13 challenge. *American Journal of Physiology-Lung Cellular and Molecular Physiology,* 291**,** L1286-L1293.

Haffner, C. D., Becherer, J. D., Boros, E. E., Cadilla, R., Carpenter, T., Cowan, D., Deaton, D. N., Guo, Y., Harrington, W., Henke, B. R., Jeune, M. R., Kaldor, I., Milliken, N., Petrov, K. G., Preugschat, F., Schulte, C., Shearer, B. G., Shearer, T., Smalley, T. L., Jr., Stewart, E. L., Stuart, J. D. & Ulrich, J. C. 2015. Discovery, Synthesis, and Biological Evaluation of Thiazoloquin(az)olin(on)es as Potent CD38 Inhibitors. *J Med Chem,* 58**,** 3548-71.

Jablonski, K. A., Gaudet, A. D., Amici, S. A., Popovich, P. G. & Guerau-De-Arellano, M. 2016. Control of the Inflammatory Macrophage Transcriptional Signature by miR-155. *PLoS One,* 11**,** e0159724.

Johnson, M. E., Mahoney, J. M., Taroni, J., Sargent, J. L., Marmarelis, E., Wu, M. R., Varga, J., Hinchcliff, M. E. & Whitfield, M. L. 2015. Experimentally-derived fibroblast gene signatures identify molecular pathways associated with distinct subsets of systemic sclerosis patients in three independent cohorts. *PLoS One,* 10**,** e0114017.

Kanamori, K. S., De Oliveira, G. C., Auxiliadora-Martins, M., Schoon, R. A., Reid, J. M. & Chini, E. N. 2018. Two Different Methods of Quantification of Oxidized Nicotinamide Adenine Dinucleotide (NAD(+)) and Reduced Nicotinamide Adenine Dinucleotide (NADH) Intracellular Levels: Enzymatic Coupled Cycling Assay and Ultra-performance Liquid Chromatography (UPLC)-Mass Spectrometry. *Bio Protoc,* 8**,** e2937.

Misharin, A. V., Morales-Nebreda, L., Mutlu, G. M., Budinger, G. R. & Perlman, H. 2013. Flow cytometric analysis of macrophages and dendritic cell subsets in the mouse lung. *Am J Respir Cell Mol Biol,* 49**,** 503-10.

Prasad, S., Neef, T., Xu, D., Podojil, J. R., Getts, D. R., Shea, L. D. & Miller, S. D. 2018. Tolerogenic Ag-PLG nanoparticles induce tregs to suppress activated diabetogenic CD4 and CD8 T cells. *J Autoimmun,* 89**,** 112-124.

Roberson, E. D. O., Cao, L., Morales-Heil, D. J., Korman, B. & Varga, J. 2016. Biomarker Identification & Molecular Sub-Classification in Systemic Sclerosis for Precision Medicine Using RNA-Seq. *Arthritis & Rheumatology,* 68.

Sargent, J. L., Li, Z., Aliprantis, A. O., Greenblatt, M., Lemaire, R., Wu, M. H., Wei, J., Taroni, J., Harris, A., Long, K. B., Burgwin, C., Artlett, C. M., Blankenhorn, E. P., Lafyatis, R., Varga, J., Clark, S. H. & Whitfield, M. L. 2016. Identification of Optimal Mouse Models of Systemic Sclerosis by Interspecies Comparative Genomics. *Arthritis Rheumatol,* 68**,** 2003-15.

Skaug, B., Khanna, D., Swindell, W. R., Hinchcliff, M. E., Frech, T. M., Steen, V. D., Hant, F. N., Gordon, J. K., Shah, A. A., Zhu, L. S., Zheng, W. J., Browning, J. L., Barron, A. M. S., Wu, M. H., Visvanathan, S., Baum, P., Franks, J. M., Whitfield, M. L., Shanmugam, V. K., Domsic, R. T., Castelino, F. V., Bernstein, E. J., Wareing, N., Lyons, M. A., Ying, J., Charles, J., Mayes, M. D. & Assassi, S. 2020. Global skin gene expression analysis of early diffuse cutaneous systemic sclerosis shows a prominent innate and adaptive inflammatory profile. *Annals of the Rheumatic Diseases,* 79**,** 379-386.

Tarrago, M. G., Chini, C. C. S., Kanamori, K. S., Warner, G. M., Caride, A., De Oliveira, G. C., Rud, M., Samani, A., Hein, K. Z., Huang, R., Jurk, D., Cho, D. S., Boslett, J. J., Miller, J. D., Zweier, J. L., Passos, J. F., Doles, J. D., Becherer, D. J. & Chini, E. N. 2018. A Potent and Specific CD38 Inhibitor Ameliorates Age-Related Metabolic Dysfunction by Reversing Tissue NAD(+) Decline. *Cell Metab,* 27**,** 1081-1095 e10.

Yokoi, H., Kasahara, M., Mori, K., Ogawa, Y., Kuwabara, T., Imamaki, H., Kawanishi, T., Koga, K., Ishii, A., Kato, Y., Mori, K. P., Toda, N., Ohno, S., Muramatsu, H., Muramatsu, T., Sugawara, A., Mukoyama, M. & Nakao, K. 2012. Pleiotrophin triggers inflammation and increased peritoneal permeability leading to peritoneal fibrosis. *Kidney Int,* 81**,** 160-9.

Yushkevich, P. A., Piven, J., Hazlett, H. C., Smith, R. G., Ho, S., Gee, J. C. & Gerig, G. 2006. User-guided 3D active contour segmentation of anatomical structures: significantly improved efficiency and reliability. *Neuroimage,* 31**,** 1116-28.